The Astrophysical Journal, 830:110 (12pp), 2016 October 20 doi:10.3847/0004-637X/830/2/110

COMPARISON OF DAMPED OSCILLATIONS IN SOLAR AND STELLAR X-RAY FLARES

I.-H. Cho[1,2], K.-S. Cho[1,2], V. M. Nakariakov[3,4,5], S. Kim[1], and P. Kumar[1]
[1] Korea Astronomy and Space Science Institute, Daejeon 305-348, Korea; kscho@kasi.re.kr
[2] University of Science and Technology, Daejeon 305-348, Korea
[3] School of Space Research, Kyung Hee University, Yongin, 446-701, Korea
[4] Centre for Fusion, Space & Astrophysics, Physics Department, University of Warwick, Coventry CV4 7AL, UK
[5] Astronomical Observatory at Pulkovo, Russian Academy of Sciences, 196140 St. Petersburg, Russia
Received 2016 May 29; revised 2016 July 29; accepted 2016 August 2; published 2016 October 17

ABSTRACT

We explore the similarity and difference of the quasi-periodic pulsations (QPPs) observed in the decay phase of solar and stellar flares at X-rays. We identified 42 solar flares with pronounced QPPs, observed with *RHESSI*, and 36 stellar flares with QPPs, observed with *XMM-Newton*. The empirical mode decomposition (EMD) method and least-squares fit by a damped sine function were applied to obtain the periods (P) and damping times (τ) of the QPPs. We found that (1) the periods and damping times of the stellar QPPs are 16.21 ± 15.86 minutes and 27.21 ± 28.73 minutes, while those of the solar QPPs are 0.90 ± 0.56 and 1.53 ± 1.10 minutes, respectively; (2) the ratios of the damping times to the periods (τ/P) observed in the stellar QPPs (1.69 ± 0.56) are statistically identical to those of solar QPPs (1.74 ± 0.77); and (3) the scalings of the QPP damping time with the period are well described by the power law in both solar and stellar cases. The power indices of the solar and stellar QPPs are 0.96 ± 0.10 and 0.98 ± 0.05, respectively. This scaling is consistent with the scalings found for standing slow magnetoacoustic and kink modes in solar coronal loops. Thus, we propose that the underlying mechanism responsible for the stellar QPPs is the natural magnetohydrodynamic oscillation in the flaring or adjacent coronal loops, as in the case of solar flares.

Key words: methods: observational – stars: low-mass – Sun: flares – Sun: oscillations

1. INTRODUCTION

X-ray light curves of solar flares contain quasi-periodic pulsations (QPPs; e.g., Nakariakov 2007; Nakariakov & Melnikov 2009), which are detected before and during the impulsive phase (e.g., Antonucci et al. 1984; Fárník et al. 2003; Inglis et al. 2008) and in the decay phase (e.g., Kim et al. 2012; Kumar et al. 2013, 2015) of the flares. QPPs are found to be a common feature of solar flaring light curves associated with both thermal (Simões et al. 2015) and nonthermal emission (Kupriyanova et al. 2010). In the impulsive phase, QPPs might be explained by a repetitive regime of spontaneous magnetic reconnection ("magnetic dripping"; see Nakariakov et al. 2010), such as periodic shedding of plasmoids (e.g., Kliem et al. 2000; Bárta et al. 2008; Kumar & Cho 2013), or by an effect of magnetohydrodynamic (MHD) oscillations: variation of the plasma and magnetic field parameters, which changes the efficiency of the gyrosynchrotron emission (e.g., Stepanov et al. 2004; Khodachenko et al. 2006; Kuznetsov et al. 2015), periodically changes the nonthermal particle kinematics (e.g., Zaitsev & Stepanov 1982), or periodically triggers magnetic reconnection by MHD oscillations (Chen & Priest 2006; Nakariakov et al. 2006). The modulating MHD oscillations could be confined to the flaring site, or could occur in plasma structures situated nearby. In particular, one possibility is the leakage of sunspot oscillations in the corona in the form of slow magnetoacoustic waves (e.g., De Moortel 2009; Reznikova & Shibasaki 2011; Sych & Nakariakov 2014; Cho et al. 2015) that reach the coronal reconnection sites and periodically trigger or modulate the process of reconnection (e.g., Chen & Priest 2006; Sych et al. 2009; Kumar et al. 2016). In the decay phase of flares, QPPs could be explained in terms of natural oscillations in the flaring loops, e.g., standing kink or slow-mode waves. These waves can be directly or indirectly excited by an impulsive source associated with the flare or CME (e.g., Aschwanden et al. 2002; Nakariakov et al. 2004; Tsiklauri et al. 2004; Selwa et al. 2005; Selwa & Ofman 2010; Zimovets & Nakariakov 2015). QPPs have been detected at many wavelengths, from radio (e.g., Wright & Nelson 1987; Qin et al. 1996; Grechnev et al. 2003; Nakariakov et al. 2003) to extreme-ultraviolet (EUV) (e.g., Wang et al. 2003), X-ray (e.g., Harrison 1987; Li & Gan 2008; Ning 2014) and gamma ray (Nakariakov et al. 2010).

An important class of oscillations observed in the decay phase of solar flares are so-called SUMER oscillations, first detected as periodic Doppler shifts with the Solar Ultraviolet Measurements of Emitted Radiation (SUMER, Wilhelm et al. 1995) in hot (>6 MK) coronal loops (e.g., Wang et al. 2002; Wang 2011). Wang et al. (2003) performed a statistical study on the 54 QPPs observed in the Doppler shift and soft X-ray intensity of the hot coronal loops and established that the oscillations have periods of 7–31 minutes with decay times of 5.7–36.8 minutes. Mariska (2006) detected similar Doppler-shift oscillations with periods of 5.5 minutes observed by the Bragg Crystal Spectrometer (BCS; Lang et al. 1992), which probed hotter plasma (~12–14 MK) compared to SUMER. Recently, the high-resolution observation with the Atmospheric Imaging Assembly (AIA; Lemen et al. 2012) on board the *Solar Dynamics Observatory* (*SDO*; Pesnell et al. 2012) showed that oscillations in the hot coronal loops are excited by an energy release at one of the footpoints of the arcade loops (Kumar et al. 2013, 2015). These observational findings are consistent with the interpretation of SUMER oscillations in terms of slow magnetoacoustic waves (Ofman & Wang 2002; Nakariakov et al. 2004; Taroyan et al. 2005).

QPPs are also frequently detected in stellar flares, e.g., in wide-band optical wavelengths (e.g., Rodono 1974; Mullan et al. 1992; Houdebine et al. 1993; Mathioudakis et al. 2003, 2006;

Anfinogentov et al. 2013), which are difficult to detect in the Sun. A systematic study of QPPs in stellar white-light flares was recently performed by Balona et al. (2015) and Pugh et al. (2016). Typically, stellar QPPs are seen as a periodic, decaying variation of the signal after the flare peak, which resembles SUMER oscillations in solar flares. Unfortunately, there is no observational example of QPPs in a solar white-light flare, so the direct comparison is difficult. However, Pugh et al. (2015) recently observed a multiperiodic oscillation in a stellar white-light flare, which supports the interpretation of stellar QPPs as natural MHD oscillations of the flaring loops.

Various aspects of stellar flares, including powerful superflares, seemed to be similar to those of solar flares (e.g., Aschwanden et al. 2008; Maehara et al. 2012). The similarity in solar and stellar flares, including the QPPs, may give us hints to understand the nature of the flares and associated oscillations, as well as coronal plasma properties for various stars, including the Sun (Balona et al. 2015; Chang et al. 2015). In particular, properties of oscillating loops could be estimated by applying an appropriate model to the frequency and amplitude modulation of the perturbation, which are independent of the sharpness and strength of the sources. Particularly, stellar X-ray flares can provide proper parameters such as the emission measure, temperature, abundance, and density of the flaring loops (e.g., Raassen et al. 2007; Pandey & Karmakar 2015), which are essential for the indirect determination of the coronal magnetic field strength. First attempts to use QPPs for stellar coronal seismology have been made by Mitra-Kraev et al. (2005), Pandey & Srivastava (2009), Anfinogentov et al. (2013), and Srivastava et al. (2013).

In this work, we perform a comparative study of QPPs in the decay phase of solar and stellar flares, aiming to establish relationships of these phenomena and reveal whether they have similar or different characteristics. To minimize a possible selection effect from different wavelengths, we consider data obtained in the energy bands 3–12 keV of *RHESSI* (Lin et al. 2002) for solar flares and 0.3–2 keV of *XMM-Newton* (Jansen et al. 2001). In this study we consider cool dwarf stars, because the envelope layers of those stars are convective and thus their coronal magnetic activities could be assumed to be similar to the Sun.

In Section 2, we describe the data sets analyzed and present the method used to detect the oscillatory patterns in the signals. In Section 3, we show the relationships between the periods and damping times observed in both solar and stellar flares. Finally, we summarize and discuss our results.

2. DATA AND METHODS

2.1. QPPs in Solar Flares

We have selected 59 events with clear QPPs in the solar X-ray flares that occurred in 2014 and were observed with *RHESSI*. This instrument was designed to investigate particle acceleration and impulsive energy releases in solar flares, delivering the imaging and spectroscopic information in X-ray/gamma-ray bands. It covers the energy range from soft X-rays, from 3 keV, up to gamma rays, 17 MeV. Figure 1 shows an example of a solar flare that occurred on 2014 October 30 at 01:33:10 UT, observed also by the *SDO*/AIA. The CLEAN algorithm is used to reconstruct the *RHESSI* image with

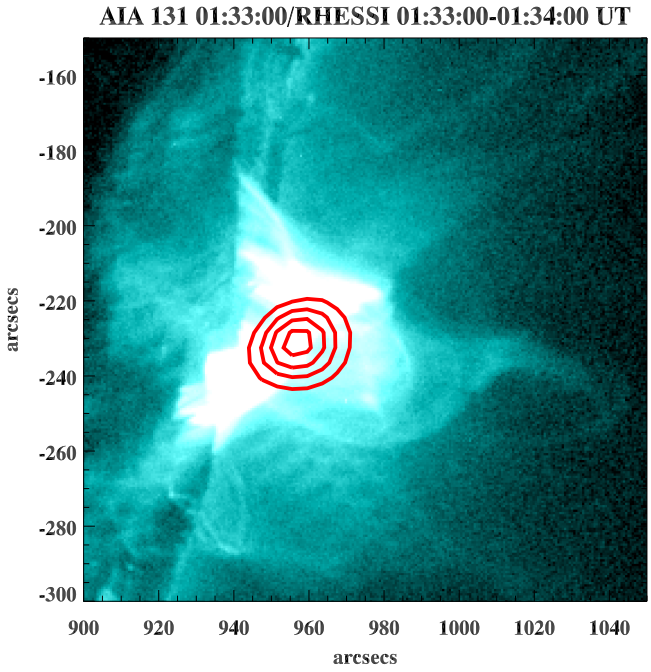

Figure 1. Example of a solar flare observed at 2014 October 30 01:33:00 UT. The red contours correspond to the 30%, 50%, 70%, and 90% count levels relative to the maximum X-ray counts measured by *RHESSI* in the 3–12 keV channel. The soft X-ray emission contours are superimposed on the EUV image obtained with *SDO*/AIA at 131 Å.

1-minute integration time (Hurford et al. 2002, and references therein). The flare locations were given by the *RHESSI* flare list.[6] Light curves were obtained by integrating the X-ray signal over the whole flaring site at 3–25 keV. First, the flare was identified in the low-energy channel, 3–6 keV, where the signal is typically the strongest, by eye. Then, if the correlation coefficient between the lowest energy signal and the signals obtained at 6–12 keV and 12–25 keV bands was higher than 0.95, those signals were also taken into consideration. The list of the flares used in this study is presented in Table 1. The first three columns represent the epochs of the flares. The fourth and fifth columns are the positions where the flares occurred.

Figure 2 shows how we detected the QPP patterns in the X-ray light curves. The top panel shows the time variation of the X-ray count rate of the flare shown in Figure 1. To detect a QPP effectively, the smooth trend should be properly removed from the signal, as it may affect the spectral behavior of the residual power spectrum (e.g., Mariska 2006; Chang 2014). We obtained the trend by applying the EMD (Huang et al. 1998). The EMD efficiently decomposes the original time series into the intrinsic mode functions (IMFs). In particular, the IMF with the slowest characteristic timescale may be used as a trend of the original signal. The advantage of this approach is its independence of any assumptions that are intrinsic in other detrending methods, for example, the spectral band and filter function of low-frequency filtering, the time duration of smoothing, the form and parameters of the best-fitting detrending function, etc. This highly adaptive method has been specifically designed for the analysis of nonlinear and nonstationary time series and has been successfully applied to the analysis of various solar and geophysical phenomena (e.g., Wu et al. 2011; Kolotkov et al. 2015a, 2015b).

In this study, the trends are defined as a sum of several lowest-frequency IMFs, allowing us to remove the steep decreasing

[6] http://hesperia.gsfc.nasa.gov/hessidata/dbase/hessi_flare_list.txt

Table 1
RHESSI Flare List for the Solar QPPs

ID	*RHESSI* Flare ID	Start Time of QPPs	X (arcsec)	Y (arcsec)	Period (minutes)	τ (minutes)	Significance Level
1	14010709	2014 Jan 07T03:35:35	−142.08	−57.37	0.903	1.118	>0.99
2	14010713	2014 Jan 07T03:52:58	−120.47	193.16	0.755	1.347	<0.70
3	14020696	2014 Feb 06T22:12:57	682.46	294.00	0.543	1.540	>0.95
4	14020697	2014 Feb 06T23:03:43	706.70	−182.74	1.172	2.061	>0.70
5	14020702	2014 Feb 07T00:36:38	700.95	−150.62	0.684	0.818	<0.70
6	14020704	2014 Feb 07T00:48:25	713.63	−182.77	0.724	1.389	>0.99
7	14021315	2014 Feb 13T05:51:37	⋯	⋯	1.765	3.788	>0.99
8	14021315	2014 Feb 13T05:52:26	⋯	⋯	0.878	1.573	>0.95
9	14021330	2014 Feb 13T06:08:05	⋯	⋯	2.074	1.904	>0.99
10	14021330	2014 Feb 13T06:08:16	⋯	⋯	0.346	0.570	>0.95
11	14021410	2014 Feb 14T02:55:21	414.43	−91.96	0.789	1.167	>0.70
12	14021410	2014 Feb 14T02:56:41	414.43	−91.96	0.377	0.574	>0.95
13	14021410	2014 Feb 14T03:04:57	414.43	−91.96	1.244	1.636	>0.70
14	14021410	2014 Feb 14T03:04:34	414.43	−91.96	0.831	1.331	>0.80
15	14021411	2014 Feb 14T03:14:60	417.46	−99.46	1.495	2.064	>0.80
16	14021417	2014 Feb 14T04:46:37	444.86	−72.86	1.015	2.018	>0.99
17	14021417	2014 Feb 14T04:47:05	444.86	−72.86	0.684	0.968	<0.70
18	14021460	2014 Feb 14T16:39:54	614.76	−104.82	0.437	0.806	>0.90
19	14021462	2014 Feb 14T17:12:16	506.00	−101.72	1.141	1.486	>0.99
20	14021462	2014 Feb 14T17:13:20	506.00	−101.72	0.564	0.635	>0.70
21	14021463	2014 Feb 14T17:23:21	512.64	−131.75	1.818	1.368	>0.99
22	14021471	2014 Feb 14T18:35:59	500.04	−95.24	1.471	2.533	>0.99
23	14022434	2014 Feb 24T12:05:31	350.59	−91.77	0.673	1.073	>0.99
24	14022434	2014 Feb 24T12:05:32	350.59	−91.77	0.346	1.253	>0.95
25	14022434	2014 Feb 24T12:16:26	350.59	−91.77	1.278	2.993	>0.99
26	14022549	2014 Feb 25T00:47:20	−925.93	−208.65	0.996	4.841	>0.80
27	14022813	2014 Feb 28T02:55:55	917.89	−170.99	0.470	0.943	>0.80
28	14022813	2014 Feb 28T02:57:03	917.89	−170.99	0.298	0.245	<0.70
29	14030843	2014 Mar 09T00:00:41	−542.15	−95.59	1.154	1.411	>0.90
30	14031016	2014 Mar 10T04:09:05	−689.42	−233.41	0.479	0.437	<0.70
31	14031019	2014 Mar 10T05:30:45	901.11	329.83	0.418	0.714	>0.95
32	14061114	2014 Jun 11T05:34:39	534.63	−197.99	0.247	0.340	>0.70
33	14061115	2014 Jun 11T05:43:42	541.50	−203.36	0.501	0.501	>0.70
34	14061115	2014 Jun 11T05:43:50	541.50	−203.36	0.342	0.434	>0.95
35	14061453	2014 Jun 14T20:17:53	883.85	−345.60	1.711	1.646	>0.90
36	14061459	2014 Jun 14T21:59:20	904.73	211.92	0.369	0.506	>0.80
37	14061462	2014 Jun 14T22:02:32	906.60	206.75	0.359	0.422	>0.95
38	14061463	2014 Jun 14T22:15:49	937.80	−213.53	2.116	3.957	>0.95
39	14102075	2014 Oct 20T20:37:48	−560.12	−326.47	0.857	1.601	>0.99
40	14102079	2014 Oct 20T21:07:38	−578.82	−270.98	0.710	0.680	>0.95
41	14102079	2014 Oct 20T21:07:48	−578.82	−270.98	0.497	0.369	>0.95
42	14102085	2014 Oct 20T22:48:37	−539.72	−304.12	0.772	2.103	>0.95
43	14102085	2014 Oct 20T22:50:08	−539.72	−304.12	0.321	0.731	>0.95
44	14102642	2014 Oct 26T10:06:24	515.23	−298.81	0.859	1.139	<0.70
45	14102643	2014 Oct 26T10:15:46	511.76	−306.18	0.668	0.927	>0.95
46	14102647	2014 Oct 26T11:56:41	526.39	−299.75	0.517	0.476	>0.99
47	14102648	2014 Oct 26T12:37:55	547.73	−299.48	2.327	3.924	>0.95
48	14102704	2014 Oct 27T01:52:35	670.07	−274.56	0.393	0.398	>0.80
49	14102704	2014 Oct 27T02:02:22	670.07	−274.56	0.902	0.949	<0.70
50	14102704	2014 Oct 27T02:02:28	670.07	−274.56	0.571	0.895	>0.95
51	14102709	2014 Oct 27T03:28:55	675.85	−277.44	0.614	1.125	>0.70
52	14102709	2014 Oct 27T03:41:54	675.85	−277.44	0.578	1.531	>0.95
53	14103003	2014 Oct 30T01:33:17	956.95	−236.79	0.478	0.623	>0.95
54	14121314	2014 Dec 13T05:57:08	872.87	−41.86	1.769	3.389	>0.99
55	14121314	2014 Dec 13T06:02:49	872.87	−41.86	0.607	0.915	>0.99
56	14121315	2014 Dec 13T06:35:31	351.13	−242.53	0.751	0.882	>0.70
57	14121773	2014 Dec 17T19:30:45	−353.72	−162.32	0.944	1.353	>0.95
58	14121773	2014 Dec 17T19:30:20	−353.72	−162.32	0.485	0.812	>0.70
59	14121776	2014 Dec 17T20:34:04	44.29	−294.75	0.394	0.708	>0.70

pattern typical for flares. The residual is the sum of the remaining IMFs. If the residual includes the IMF that shows a damped oscillatory pattern, it was fitted with a damped harmonic function, $I = A \exp[-(t - t_0)/\tau]\sin[(t - t_0)/P - B]$, where A, t_0, and B are the amplitude, starting time, and phase of the oscillation, respectively. We set the starting time of the sine function equal to

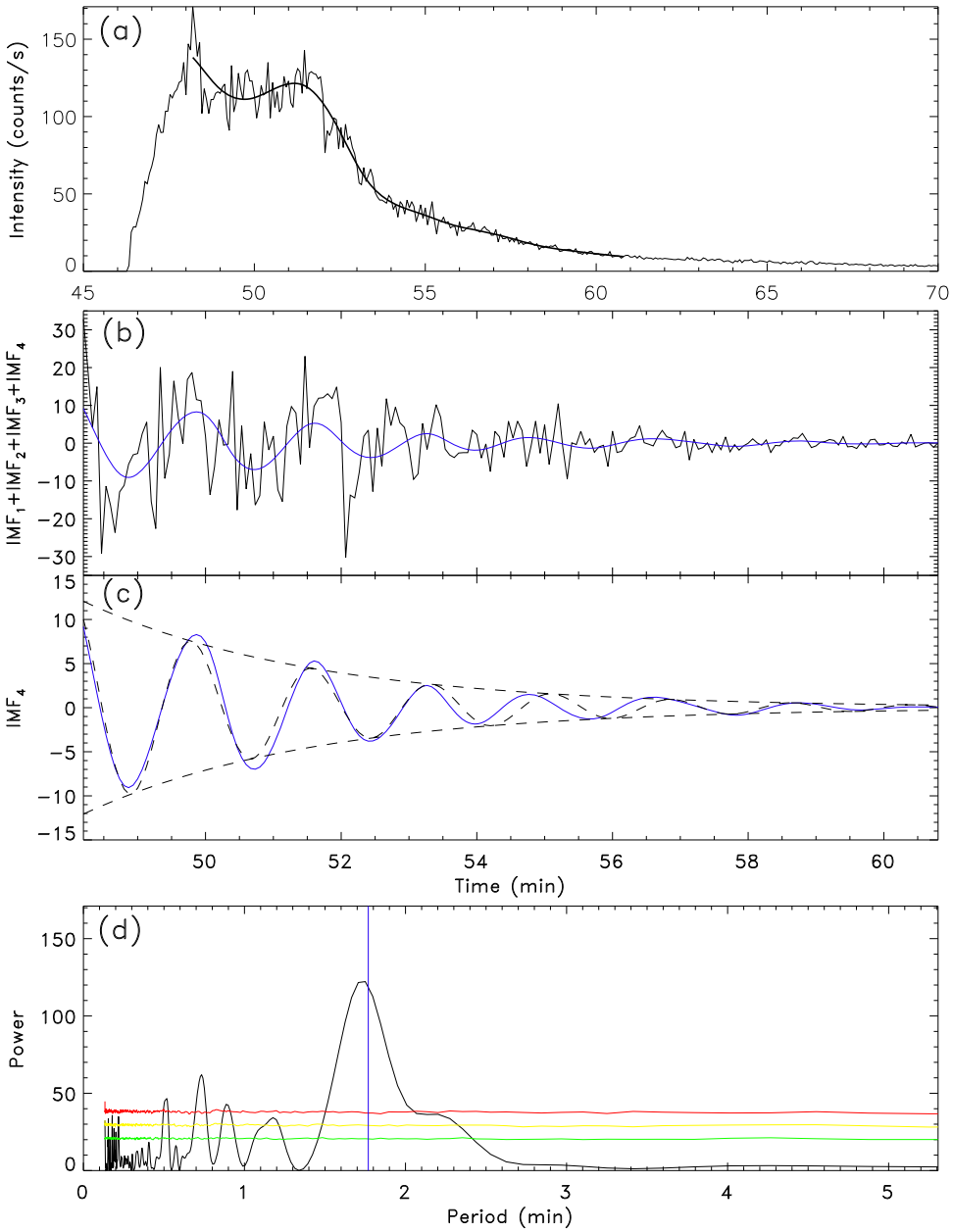

Figure 2. (a) Example of an X-ray light curve of a solar flare observed with *RHESSI* at the 3–24 keV energies. The smoothed solid line is the trend obtained by applying the EMD technique. (b) Residual signal obtained by detrending, consisting of several IMFs. The blue curve shows the damped oscillatory IMF. (c) Best fitting of the IMF by a decaying harmonic oscillation (the black dashed curve). (d) Power spectrum of the residual signal given in panel (b). The blue vertical line is the period obtained from fitting by the least-squares technique. The red, yellow, and green curves are 99%, 95%, and 90% confidence intervals, respectively.

the starting time of the exponential function, which was after the flare peak time, by adjusting the initial values. In panel (b), the residual (black) and the best-fitting QPP (blue) are presented. The best-fitting curve is shown by the dashed line in panel (c). Panel (d) shows the power spectrum of the residual. Because the EMD always produces the quasi-periodic signals for the IMFs, the obtained period of the damped sine function should be tested by calculating the residual power spectrum. The vertical line in this panel is the period obtained from the damped sine fitting. The red, yellow, and green lines are the 99%, 95%, and 90% confidence intervals, respectively. The significance is defined by the Fisher randomization method (Linnell Nemec & Nemec 1985; O'Shea et al. 2001; Yuan et al. 2011; Yu et al. 2013). The confidence interval for each frequency is determined from the cumulative probability of the 10,000 noise powers at each frequency. The peak periods in the power spectra are slightly different from periods of the best-fitting curve. It may be attributed to the nonlinear nature of the QPPs. However, we checked whether the fitted periods are within the half width of the significant peaks in the power spectrum and found that in the majority of the analyzed light curves, most of the best-fitting periods satisfied this condition. The periods and damping times with the significance levels estimated in the solar QPPs are presented in Table 1.

Figure 3 shows the fitting results for QPPs in all 59 solar flares. The number in each panel denotes the flare ID in Table 1. The horizontal and vertical scales are normalized by the damping time and amplitude of the exponentially

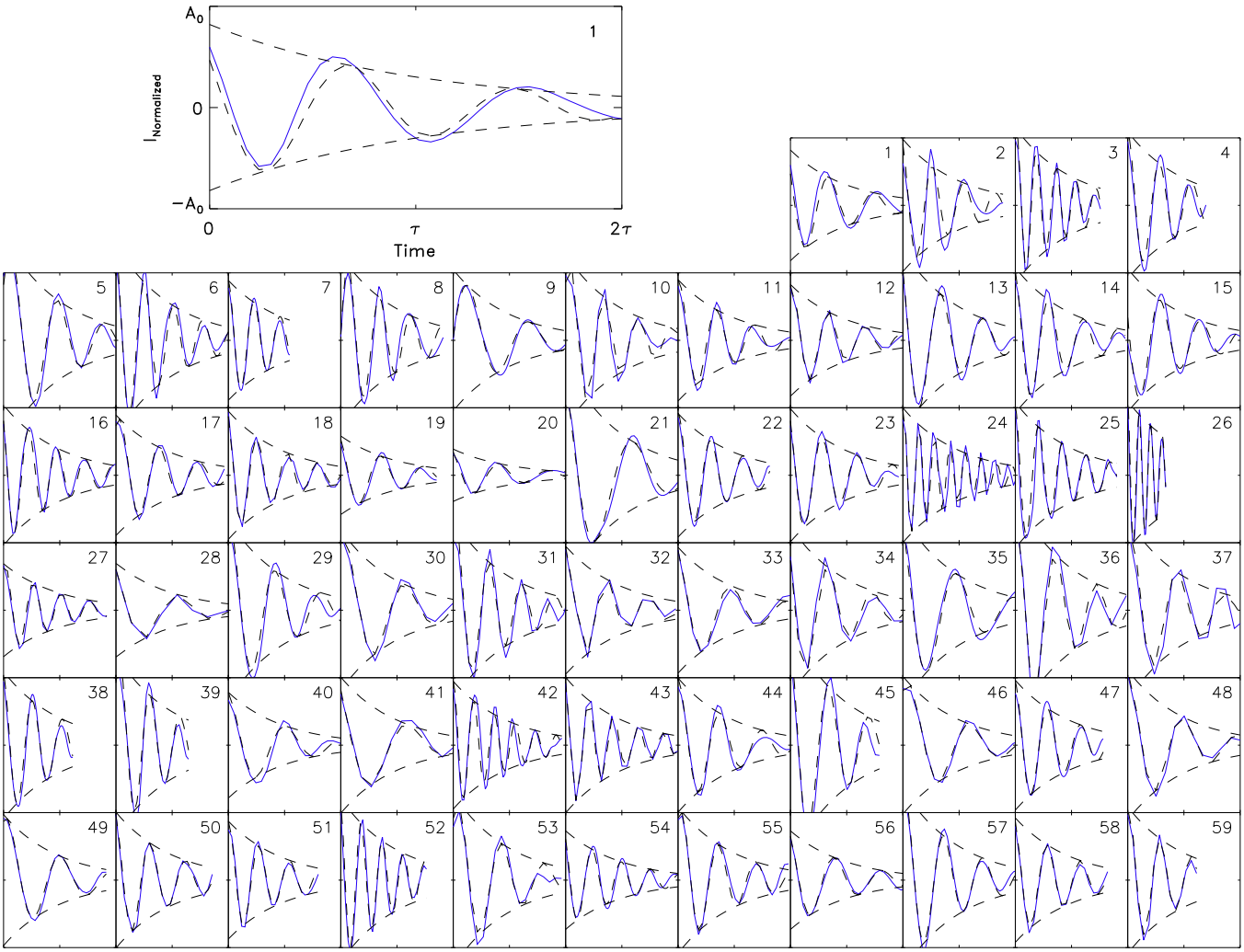

Figure 3. The 59 candidates for the solar flaring QPPs (blue) with their damped harmonic fit (dashed). The scales of the horizontal and vertical axes are normalized to the maximum amplitudes of the exponential function and damping times, respectively, as shown in the zoomed-in plot of the first sample.

decaying harmonic functions, respectively, as shown in the enlarged version of flare #1. The scales of the horizontal and vertical axes in all small panels are omitted for visualization purposes. Each panel is similar to the plot shown in Figure 2(c).

2.2. QPPs in Stellar Flares

We also selected 52 QPPs in light curves of stellar X-ray flares detected in the 0.3–2 keV band of *XMM-Newton*. The telescope includes the European Photon Imaging Camera (EPIC; Strüder et al. 2001; Turner et al. 2001), the Reflection Grating Spectrometer (RGS; den Herder et al. 2001), and the Optical Monitor (OM; Mason et al. 2001). EPIC consists of pn-CCD (0.15–15 keV) and two MOS-CCDs (0.1–10 keV), which almost continuously registers photons as events. The mean time cadence of light curves is about 60 s, ranging from 10 to 300 s. The cadence time was not the same for different flares. The original time cadence of *XMM-Newton* data is less than 1 s, but to improve the signal-to-noise ratio, we binned the data. To determine the appropriate binning time, we first applied the 60 s binning. If the data still looked too noisy, we then applied a longer time binning, e.g., 120 s, and so on, until the binned data are not too noisy. This approach led to different binning times for different events.

Our targets include 16 dwarf stars (CN Leo, HD179949, YZ Canis Minoris, 47 Cas, GJ 674, HD 189733, AU Mic, 61 Cyg, LP412-31, Proxima Cen, ξ Boo, YY Gem, Ross 154, At Mic, κ^1 Cet, and SCR J1845-6357), two binary dwarfs with a white dwarf as a companion (V471 Tauri and AE Aqr), and four serendipitous flares in the open clusters (Zeta Orion, BL Hyi, IC2602, and Blanco 1). All of these targets are known either as flare-producing stars or as having flare-producing companions (Choi et al. 1999; Robinson et al. 1999; Tsikoudi & Kellett 2000; Güdel et al. 2001, 2004; Magee et al. 2003; Trenholme et al. 2004; Shkolnik et al. 2005; Stelzer et al. 2006; Stepanov et al. 2006; Watson et al. 2006; Pandey & Singh 2008; Liefke et al. 2010; Pillitteri et al. 2010, 2014; Robrade et al. 2010, 2012; Fuhrmeister et al. 2011; Scandariato et al. 2013; Bhatt et al. 2014; Pandey & Karmakar 2015). The list of targets, including *XMM-Newton* ObsID with its source and background regions used for the light-curve extractions, are given in Table 2.

The light curves are extracted by using the *XMM-Newton* Science Analysis System (SAS[7]) version 14.0. We only use the

[7] http://heasarc.gsfc.nasa.gov/docs/xmm/abc/

Table 2
XMM-Newton Target List of the Stellar QPPs

ID	Target ID	Start Time QPPs	Source Region[a]	Background Region[a]	Period (minutes)	τ (minutes)	Significance Level
1	0200530701	2006 May 22T01:03:28	26365, 27957, 0, 600	27365, 25957, 600	2.819	4.738	>0.90
2	0605581001	2009 Oct 07T05:20:37	27240, 27401, 300	27240, 27401, 300, 500	55.677	111.966	>0.80
3	0602290101	2009 May 06T23:11:50	26415, 27947, 0, 600	24415, 29947, 600	57.774	71.784	<0.70
4	0111460101	2000 Oct 09T14:20:43	24987, 24162, 100, 800	25687, 27662, 800	7.041	12.963	<0.70
5	0111520101	2001 Sep 11T06:38:13	23904, 25690, 75, 600	25204, 29190, 600	5.544	11.298	>0.70
6	0551020101	2008 Sep 05T17:32:38	27083, 27641, 0, 500	26083, 25641, 500	15.071	21.933	>0.80
7	0672390201	2011 May 01T06:35:43	24304, 24486, 0, 300	25304, 25486, 300	10.276	11.415	<0.70
8	0672390201	2011 May 01T06:35:43	24304, 24486, 0, 300	25304, 25486, 300	18.383	36.919	>0.80
9	0111420101	2000 Oct 14T06:06:52	27525, 27113, 120, 800	28525, 23613, 800	8.560	11.815	>0.70
10	0111420101	2000 Oct 13T17:33:52	27525, 27113, 120, 800	28525, 23613, 800	8.543	27.472	<0.70
11	0111420101	2000 Oct 13T17:33:52	27525, 27113, 120, 800	28525, 23613, 800	15.516	21.832	>0.70
12	0111420101	2000 Oct 13T17:21:52	27525, 27113, 120, 800	28525, 23613, 800	5.237	9.405	>0.80
13	0112530101	2002 Sep 15T22:28:04	22517, 19333, 0, 400	22517, 19333, 500, 700	51.783	70.107	>0.95
14	0041741101	2004 May 01T16:21:50	23959, 24366, 300	23261, 23661, 300	24.542	35.333	>0.95
15	0300170101	2006 Feb 19T10:05:38	27398, 27296, 0, 500	27898, 25796, 500	3.011	4.352	>0.80
16	0300170101	2006 Feb 19T10:05:38	27398, 27296, 0, 500	27898, 25796, 500	5.171	7.674	>0.90
17	0300170101	2006 Feb 19T10:05:38	27398, 27296, 0, 500	27898, 25796, 500	7.552	17.107	>0.90
18	0300170101	2006 Feb 19T10:05:38	27398, 27296, 0, 500	27898, 25796, 500	13.935	16.468	>0.99
19	0143630101	2004 Nov 03T01:27:28	26575, 27303, 0, 350	27575, 26303, 300	10.904	16.910	>0.99
20	0143630101	2004 Nov 03T01:27:28	26575, 27303, 0, 350	27575, 26303, 300	20.213	41.386	<0.70
21	0049350101	2001 Aug 12T18:08:42	26761, 27721, 200, 800	26661, 24221, 600	11.127	23.597	>0.95
22	0049350101	2001 Aug 12T18:26:42	26761, 27721, 200, 800	26661, 24221, 600	18.161	33.608	>0.99
23	0056030101	2001 Jan 19T16:58:52	25335, 23878, 0, 500	25335, 23878, 1000, 1200	11.854	13.203	<0.70
24	0056030101	2001 Jan 19T18:48:52	25335, 23878, 0, 500	25335, 23878, 1000, 1200	22.120	29.424	<0.70
25	0056030101	2001 Jan 19T17:00:32	25335, 23878, 0, 500	25335, 23878, 1000, 1200	20.339	30.948	>0.90
26	0551120201	2009 Mar 12T10:32:29	26293, 23785, 0, 700	24293, 26285, 700	19.745	27.211	>0.95
27	0551120201	2009 Mar 12T07:22:29	26293, 23785, 0, 700	24293, 26285, 700	6.024	5.811	>0.80
28	0203260101	2004 Aug 01T12:14:47	24232, 24428, 50, 400	23232, 28428, 400	34.487	76.098	>0.90
29	0101440201	2002 Aug 13T11:56:41	24126, 26954, 0, 700	26021, 27451, 700	30.720	29.170	>0.95
30	0551120401	2009 Mar 14T07:10:07	26410, 23921, 0, 1000	23910, 26421, 1000	3.707	6.424	>0.90
31	0551120401	2009 Mar 14T07:10:07	26410, 23921, 0, 1000	23910, 26421, 1000	12.264	16.503	>0.95
32	0551120401	2009 Mar 14T07:10:07	26410, 23921, 0, 1000	23910, 26421, 1000	21.025	19.263	>0.95
33	0111180201	2001 Nov 08T04:08:37	27733, 27228, 150, 800	29251, 29691, 800	2.129	3.490	>0.90
34	0111180201	2001 Nov 08T03:57:37	27733, 27228, 150, 800	29251, 29691, 800	8.821	35.887	>0.99
35	0112880801	2000 Sep 30T01:18:07	25381, 23911, 0, 600	26881, 20911, 600	19.356	37.853	<0.70
36	0112880801	2000 Sep 30T01:19:47	25381, 23911, 0, 600	26881, 20911, 600	36.740	50.015	>0.95
37	0200530301	2005 Dec 11T09:21:41	26008, 23596, 0, 600	25008, 26596, 600	9.062	9.670	>0.95
38	0200530501	2006 May 20T02:49:48	26375, 27948, 0, 600	27375, 24948, 600	2.384	4.576	>0.99
39	0200530501	2006 May 20T00:47:38	26375, 27948, 0, 600	27375, 24948, 600	1.690	3.434	>0.90
40	0200530501	2006 May 20T00:47:08	26375, 27948, 0, 600	27375, 24948, 600	2.611	4.898	>0.95
41	0123710101	2000 Apr 25T04:50:38	26590, 27922, 75, 800	28790, 25122, 800	8.025	13.222	>0.80
42	0148440101	2002 Dec 17T01:27:20	31082, 12632, 0, 200	31082, 13632, 150	19.920	16.000	<0.70
43	0601950101	2010 Mar 20T00:46:02	24545, 24459, 100, 700	23045, 27959, 700	7.899	10.854	>0.95
44	0551120301	2009 Mar 10T03:46:59	26171, 23861, 0, 700	24671, 26361, 700	8.358	15.876	>0.99
45	0041750101	2002 Jun 16T00:56:54	21977, 19169, 0, 200	20869, 18565, 200	64.965	114.735	>0.80
46	0041750101	2002 Jun 15T21:13:34	21977, 19169, 0, 200	20869, 18565, 200	69.537	74.508	>0.70
47	0111510101	2000 Oct 16T06:34:41	27480, 27081, 75, 800	27980, 24081, 800	8.641	15.956	>0.80
48	0111510101	2000 Oct 16T06:34:41	27480, 27081, 75, 800	27980, 24081, 800	13.402	18.012	<0.70
49	0200530801	2006 May 05 24T00:34:58	26322, 27936, 0, 400	26322, 26436, 400	1.965	2.539	>0.95
50	0111410101	2002 Feb 09T22:09:31	27483, 27159, 0, 800	27483, 27159, 800, 1100	28.572	72.771	>0.90
51	0111410101	2002 Feb 09T22:09:31	27483, 27159, 0, 800	27483, 27159, 800, 1100	52.055	94.302	>0.70
52	0551022901	2008 Sep 06T08:47:09	27536, 27082, 0, 250	26536, 27082, 250	2.452	3.625	<0.70

Note.
[a] Annulus (X, Y, R_1, R_2) or in circle (X, Y, R).

0.3–2 keV energy band to avoid emission associated with nonthermal particles (e.g., Pandey & Karmakar 2015). For preprocessing, the SAS task `em(p)roc` was used. The source and background light curves were obtained by using the SAS `evselect`. The light-curve corrections are performed by using the SAS `epiclccorr`. The source regions were selected as annuli to avoid the pileup effect due to photons from a bright source. The inner radius of the annulus is determined after checking the energy spectrum by using the SAS `epatplot`. If the data sets are free from the pileup effect, we use the circle for the source region. The background region is selected in the same CCD where the source region was defined.

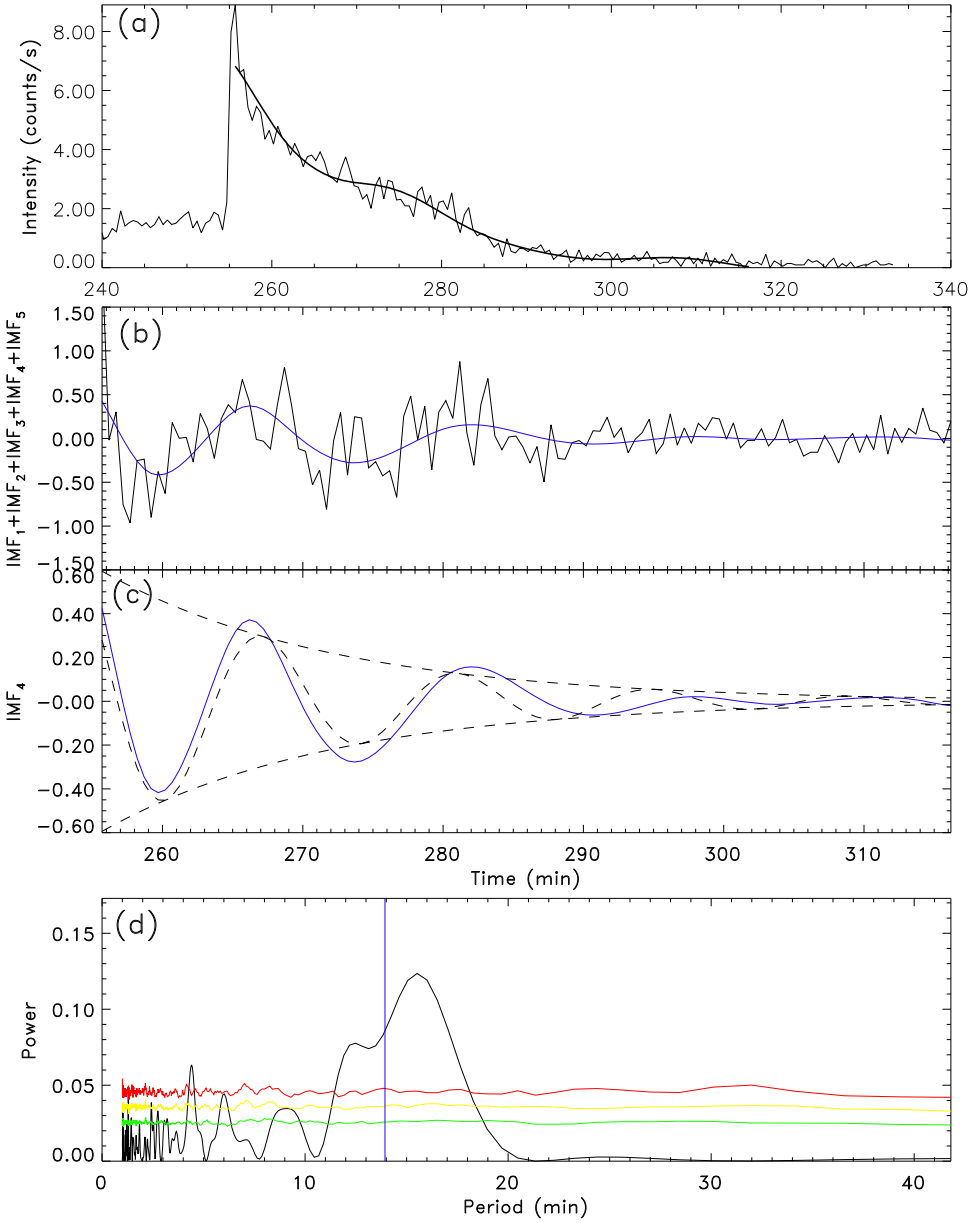

Figure 4. (a) Example of an *XMM-Newton* light curve with the smooth trend (solid curve) obtained by applying the EMD technique. (b) Residual signal obtained by detrending, consisting of several IMFs. The blue curve shows the damped oscillatory IMF. (c) Best fitting of the IMF by a decaying harmonic oscillation (the black dashed curve). (d) Power spectrum of the residual signal given in panel (b). The blue vertical line is the period obtained by best fitting. The red, yellow, and green curves are 99%, 95%, and 90% confidence intervals, respectively.

The analysis of QPPs in the stellar flare light curves was performed similarly to the solar flare analysis (Section 2.1). Figure 4 shows the analysis of a typical stellar flare that occurred at the M8 dwarf LP412-31. Panel (a) shows the X-ray light curve with the trend. Panel (b) gives the residual and the damped oscillatory IMF. Panel (c) shows the comparison of the damped oscillatory IMF with the best-fitting damped harmonic curve. Panel (d) shows the power spectrum of the residual. QPP patterns detected in 52 stellar flares are demonstrated in Figure 5. The number in each panel corresponds to the Flare ID in Table 2. The determined periods, damping times, and significance levels are also presented in Table 2.

3. RESULTS

Figure 6 shows the histograms of the periods (top), damping times (middle), and their ratios that can be considered as the quality factors (bottom), found in the analyzed solar and stellar QPPs. The cases with the detection of a periodicity above the confidence level higher than 80% were considered as significant. The insignificant samples were excluded from the further analysis. The vertical dashed lines in each panel indicate mean values of the periods, damping times, and their ratios obtained for the 42 solar and 36 stellar flares in which the detected QPPs were significant. Thus, the significant detected periods in the solar and stellar QPPs are 0.90 ± 0.56 minutes and 16.21 ± 15.86 minutes, respectively. The damping times

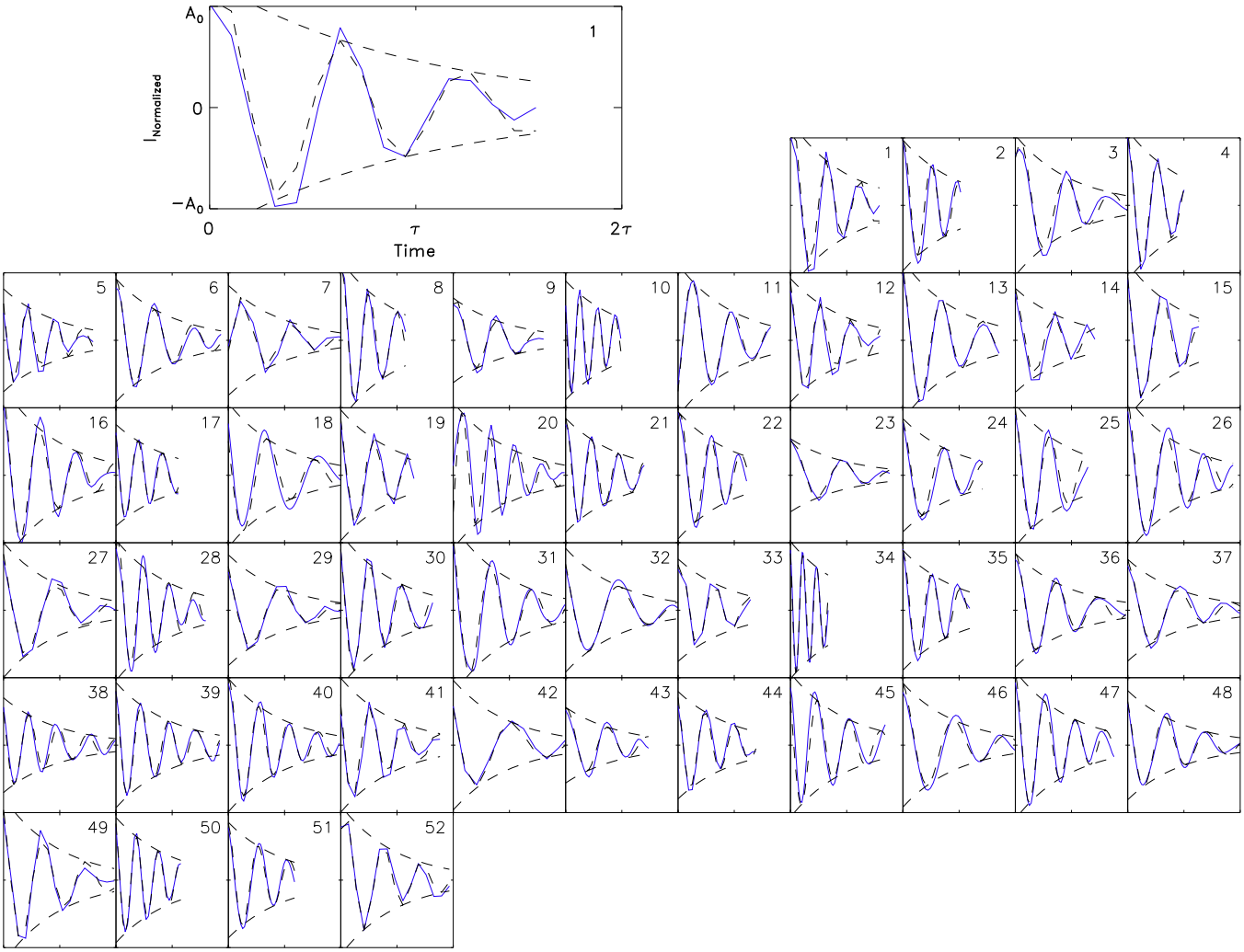

Figure 5. QPPs in stellar flares (blue) and the best-fitting damped harmonic functions (dashed). For visualization, the scales of the horizontal and vertical axes are normalized to the maximum amplitudes of the exponential function and damping times, as shown in the zoomed-in plot for the first sample.

are 1.53 ± 1.10 minutes and 27.21 ± 28.73 minutes, respectively. The overall shapes of the distributions observed in the solar and stellar QPPs are similar to each other. The characteristic scales of the periods and damping times detected in the stellar QPPs are much longer than the solar QPPs. The quantitative difference may come from the different lengths and temperatures of the stellar coronal loops. On the other hand, the ratios of the damping times τ to the periods P of the solar and stellar QPPs are $\tau/P = 1.74 \pm 0.77$ and 1.69 ± 0.56, respectively, which seem to be identical. To check whether they are the same or not, we performed the statistical Kolmogorov–Smirnov (K-S) test. The p-value of the K-S test is 0.93, which cannot reject the null hypothesis that the two distributions of the τ/P observed in the solar and stellar QPPs are the same. The statistics of the periods and damping times are presented in Table 3.

Figure 7 shows the scaling of the damping times and periods observed in both the solar (left) and stellar (right) QPPs. The best-fitting straight lines in the left and right panels are the power-law dependencies $\tau = 1.59 \pm 1.07P^{0.96\pm0.10}$ and $\tau = 1.70 \pm 1.13P^{0.98\pm0.05}$, respectively. Both power-law indices are comparable with those observed in the transverse and longitudinal oscillations of the solar flaring or coronal loops in the previous studies (see Ofman & Wang 2002; Wang et al. 2003; Goddard et al. 2016). In Figure 8, we plot the damping times as a function of the periods for both solar and stellar QPPs. The black straight line is $\tau = 1.62 \pm 1.05P^{0.99\pm0.03}$, which is obtained from the joint, solar and stellar scaling.

4. CONCLUSION AND DISCUSSION

Analysis of soft X-ray light curves of solar and stellar flares by applying the EMD method revealed the presence of 42 QPPs in solar flares and 36 QPPs in stellar flares. We performed the least-squares fitting of the detected oscillatory patterns with the damped harmonic function to the QPPs, allowing us to estimate the periods (P) and damping times (τ) of the QPPs. Most of the periods determined by fitting are well matched with the peak periods in the power spectra of the detrended light curves. We found that the periods and damping times of stellar QPPs are 16.21 ± 15.86 minutes and 27.21 ± 28.73 minutes, respectively. These values are larger than those obtained in solar QPPs of 0.90 ± 0.56 minutes and 1.53 ± 1.10 minutes. The ratios (τ/P) of the solar (1.74 ± 0.77) and stellar (1.69 ± 0.56) QPPs are found to be statistically identical.

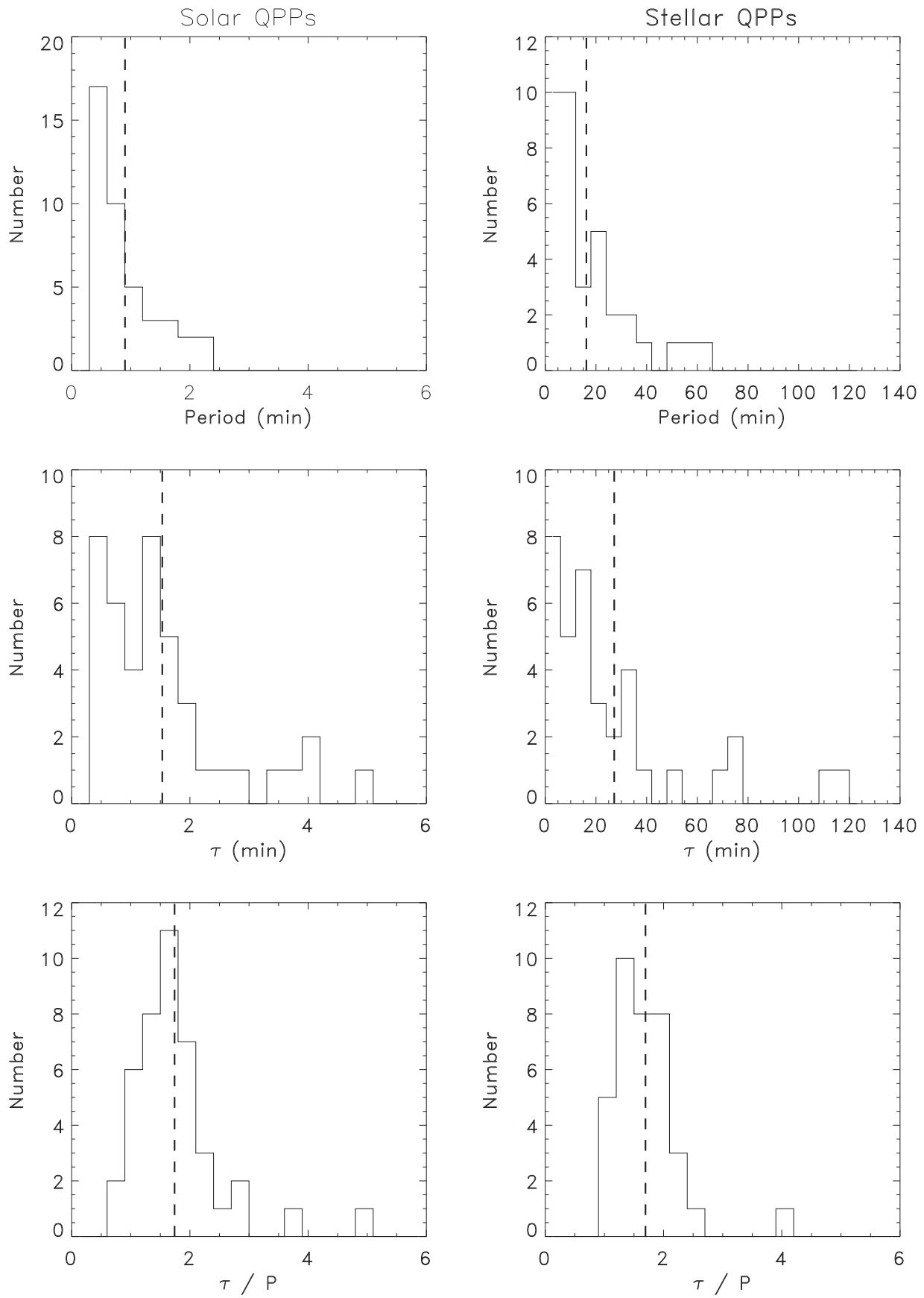

Figure 6. Distributions of the periods, damping times, and their ratios for the solar (left) and stellar (right) QPPs. Vertical dashed lines in each panel indicate their mean values.

Table 3
Statistics of the Period and Damping Time

Parameter	Solar QPPs	Stellar QPPs	K-S Test
P (minutes)	0.90 ± 0.56	16.21 ± 15.86	⋯
τ (minutes)	1.53 ± 1.10	27.21 ± 28.73	⋯
τ/P	1.74 ± 0.77	1.69 ± 0.56	p-value $= 0.93$[a]

Note.
[a] The small p-value (e.g., 0.01) indicates that the cumulative distributions are significantly different from each other.

We found that the scalings of the damping time τ with the oscillation period (P) are well fitted with a power-law dependency in the form $\tau = aP^b$ in both the solar and stellar QPPs. The amplitudes a for solar and stellar flares are found to be 1.59 ± 1.07 and 1.70 ± 1.13, respectively. The power indices b for solar and stellar flares are 0.96 ± 0.10 and 0.98 ± 0.05, respectively. These values are very close to each other and also comparable with the values observed in the solar coronal loop oscillations. For example, Wang et al. (2003) reported that the power index was 1.06 ± 0.18 in a set of 49 slow magnetoacoustic standing (SUMER) oscillations in coronal loops. Ofman & Wang (2002) found the power index to be 1.17 ± 0.34 in a set of 11 transverse loop oscillations. Thus, the main result of this study is the apparent similarity of the scaling laws of the damping times and periods of QPPs in solar and stellar flares. This finding indicates that the underlying mechanism responsible for stellar QPPs detected in the soft X-ray emission after the flare peaks is likely to be of the same nature as in solar flares and could be the natural magnetoacoustic oscillations of the flaring or adjacent coronal loops. A similar conclusion has recently been drawn by Pugh et al. (2015), based on the detection of multiple periodicities in a stellar flare. However, that result was obtained in the white-light band, which makes direct comparison with solar flares difficult. In contrast, our results are obtained in the soft X-ray band, which is a commonly used band for the detection of solar flares, allowing for the direct comparison of solar and stellar results.

The periods obtained in the solar QPPs in our study are much shorter than the periods of the slow-mode standing wave obtained by Wang et al. (2003), 7–31 minutes. The discrepancy may come from the selection effect of the instruments, as explained by Wang (2011). The *RHESSI* energy band (3–25 keV) used in this study is associated with hotter loops (Caspi et al. 2014; Ryan et al. 2014) compared to the SUMER oscillation loops, which can result in the higher sound speeds. Moreover, typically the flaring loops are much shorter than the long loops hosting SUMER oscillations, and it also contributes to the decrease in the periods of slow modes detected in soft X-rays. In addition, in flaring loops the slow oscillations may be on the second longitudinal harmonic, if they are excited simultaneously at both footpoints, e.g., by the precipitating nonthermal electrons going down from the reconnection cite along the legs of the loop (e.g., Nakariakov et al. 2004). The second harmonics have oscillation periods about two times shorter than those of the fundamental mode. Thus, it is natural to expect that soft X-ray QPPs are of shorter periods than EUV QPPs. We would also point out that our results are consistent with the 9.6–61.6 s intensity oscillations in the coronal loops observed by the Soft X-ray Telescope (SXT) on *Yohkoh*, reported by McKenzie & Mullan (1997).

In general, QPPs in flares could be produced by several different mechanisms. These mechanisms could be roughly divided into three groups: the modulation of the emitting plasma or the kinematics of nonthermal electrons by an MHD oscillation and a quasi-periodic regime of magnetic reconnection, induced by an MHD oscillation, and a spontaneous quasi-periodic magnetic reconnection—"magnetic dripping" (see Nakariakov et al. 2016, for a recent review). The apparent similarity of the time profiles of the QPPs detected in this study, the rapidly exponentially decaying trains of oscillations, with the properties of MHD oscillations observed with high spatial resolution in solar coronal plasma structures indicates that the observed QPPs are likely to be associated with MHD oscillations.

The recent study of Inglis et al. (2015) showed the importance of accounting for the effect of colored noise in the determination of the statistical significance of the spectral peaks associated with QPPs. However, Simões et al. (2015) demonstrated that QPPs are present in 80% of X-class solar flares in Cycle 24. In our study we concentrate on the QPP signals that have a specific shape, namely, the rapidly decaying harmonic oscillations. The search for a signal of this specific shape is motivated by the unequivocal detection of such signals in solar coronal observations with high spatial resolution (e.g., Kumar et al. 2015; Zimovets & Nakariakov 2015). This approach reduces significantly the false detection probability, as in this work we also account for the phase information, making our findings more robust.

Observations of stellar flares are intrinsically unimaged; hence, it is impossible to estimate directly one of the key parameters of a coronal MHD oscillation, its wavelength, by the length of the oscillating loop. However, the use of certain scalings could provide some useful, order-of-magnitude estimations (e.g., Mullan et al. 2006), linking the flaring loop length with the emission measure and the decay time of the flare. It should be done on an ad hoc basis, as the same star may have flares in active regions of quite different geometrical sizes, as one can see in solar flares. Likewise, the estimations of flaring loop lengths in Mullan et al. (2006) show a rather broad range too, for example, for the analyzed flares on AD Leo, the lengths range from 37 to 340 Mm. Nevertheless, the use of such a technique in combination with the seismological technique is an interesting topic for a follow-up study. We speculate that the flaring emission comes from a small region in the vicinity of the flare site, as is observed in solar flares. More specifically, the soft X-ray emission studied here comes from a flaring loop or arcade. As the detected periods of stellar QPPs are systematically longer than those of solar QPPs, and as the temperature of the emitting plasma is not likely to differ by more than a factor of 5, making the sound speed about two times higher maximum than in the solar flares, we may conclude that the lengths of the stellar flare loops are typically longer than in solar flares.

Several previous seismological studies for stellar QPPs gave insight into identifying the MHD mode responsible for the QPPs. For example, Mitra-Kraev et al. (2005) interpreted the soft X-ray QPP in a flare of the dwarf AT Mic as a standing slow magnetoacoustic oscillation. This interpretation allowed the authors to estimate the temperature of the flaring loop as 13 MK. Srivastava et al. (2013) observed multiple QPPs in a flare on the Proxima Cen. The measured temperature of the oscillating region was 7.2 MK. The authors interpreted the

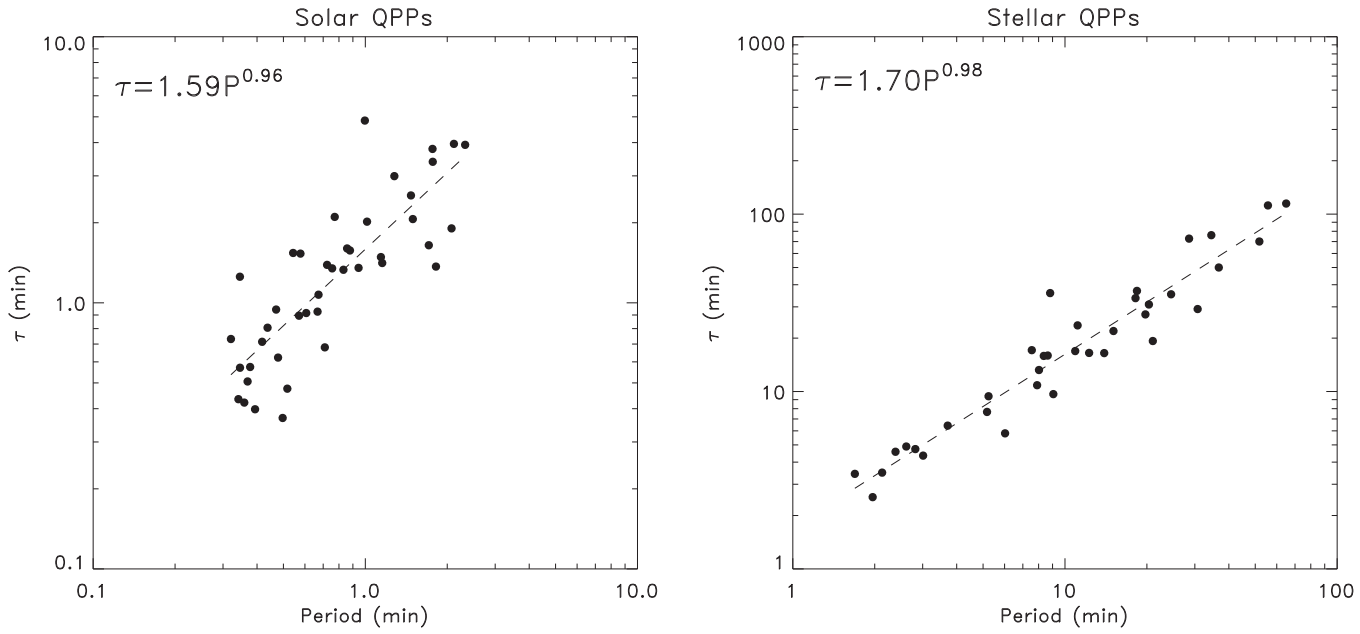

Figure 7. Damping times as a function of the period for solar (left) and stellar QPPs (right). The dashed lines show the least-squares power-law fits.

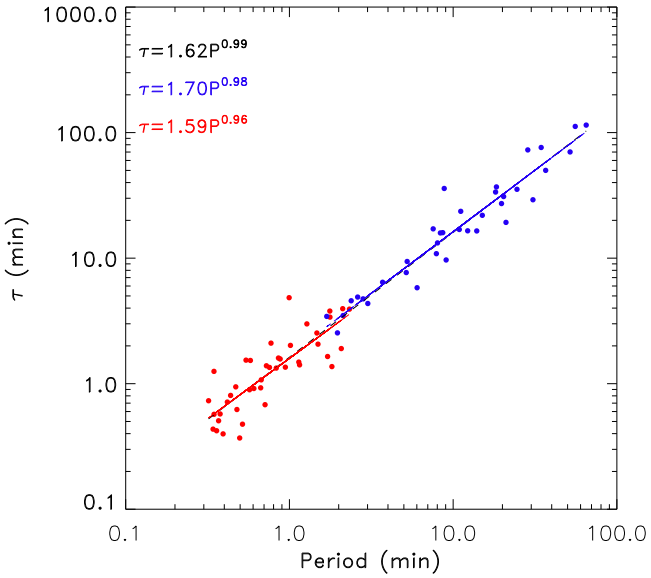

Figure 8. Damping times as a function of the period for the solar (red) and stellar QPPs (blue). The blue and red straight lines show the best-fitting power-law dependency. The black dashed line is the least-squares fit with the form of $\tau = 1.62 \times P^{0.99}$, where P and τ are periods and damping times, respectively, of the combined, solar and stellar, sets of QPPs.

QPP as a standing slow magnetoacoustic wave in the flaring loop. Pandey & Srivastava (2009) observed a QPP in a flare on the dwarf ξ Boo and interpreted it as a kink oscillation. The loop length was estimated as 380 Mm, with the mean magnetic field of 36 G. (Un)fortunately, our study does not allow us to discriminate between the longitudinal and transverse oscillations, as in the solar case the power indices of the scaling of the decay time with oscillation periods are almost identical. Therefore, we leave this issue for a follow-up study.

The variety of the timescales in the periods and damping times observed in the stars may reflect the variety of the properties of the stellar coronae such as the temperatures or lengths of the oscillating loops. More quantitative estimation can be made with the use of spectral observations, which is beyond the scope of our study.

This work is supported by the "Planetary System Research for Space Exploration" from the Korea Astronomy and Space Science Institute. V.M.N. is supported by the European Research Council under project no. 321141 SeismoSun and the BK21 plus program of the National Research Foundation funded by the Ministry of Education of Korea. We appreciate comments from the anonymous referee that improved the manuscript.

REFERENCES

Anfinogentov, S., Nakariakov, V. M., Mathioudakis, M., et al. 2013, ApJ, 773, 156
Antonucci, E., Gabriel, A. H., & Patchett, B. E. 1984, SoPh, 93, 85
Aschwanden, M. J., de Pontieu, B., Schrijver, C. J., & Title, A. M. 2002, SoPh, 206, 99
Aschwanden, M. J., Stern, R. A., & Güdel, M. 2008, ApJ, 672, 659
Balona, L. A., Broomhall, A.-M., Kosovichev, A., et al. 2015, MNRAS, 450, 956
Bárta, M., Karlický, M., & Žemlička., R. 2008, SoPh, 253, 173
Bhatt, H., Pandey, J. C., Singh, K. P., et al. 2014, JApA, 35, 39
Caspi, A., Krucker, S., & Lin, R. P. 2014, ApJ, 781, 43
Chang, H.-Y. 2014, PASJ, 66, 86
Chang, S.-W., Byun, Y.-I., & Hartman, J. D. 2015, ApJ, 814, 35
Chen, P. F., & Priest, E. R. 2006, SoPh, 238, 313
Cho, K.-S., Bong, S.-C., Nakariakov, V. M., et al. 2015, ApJ, 802, 45
Choi, C.-S., Dotani, T., & Agrawal, P. C. 1999, ApJ, 525, 399
De Moortel, I. 2009, SSRv, 149, 65
den Herder, J. W., Brinkman, A. C., Kahn, S. M., et al. 2001, A&A, 365L, 7
Fárník, F., Karlický, M., & Švestka, Z 2003, SoPh, 218, 183
Fuhrmeister, B., Lalitha, S., Poppenhaeger, K., et al. 2011, A&A, 534, 133
Goddard, C. R., Nisticò, G., Nakariakov, V. M., & Zimovets, I. V. 2016, A&A, 585, A137
Grechnev, V. V., White, S. M., & Kundu, M. R. 2003, ApJ, 588, 1163
Güdel, M., Audard, M., Magee, H., et al. 2001, A&A, 365, 344
Güdel, M., Audard, M., Reale, F., et al. 2004, A&A, 416, 713
Harrison, R. A. 1987, A&A, 182, 337
Houdebine, E. R., Foing, B. H., Doyle, J. G., & Rodono, M. 1993, A&A, 274, 245
Huang, N. E., Shen, Z., Long, S. R., et al. 1998, RSPSA, 454, 903

Hurford, G. J., Schmahl, E. J., Schwartz, R. A., et al. 2002, SoPh, 210, 61
Inglis, A. R., Ireland, J., & Dominique, M. 2015, ApJ, 798, 108
Inglis, A. R., Nakariakov, V. M., & Melnikov, V. F. 2008, A&A, 487, 1147
Jansen, F., Lumb, D., Altieri, B., et al. 2001, A&A, 365L, 1
Khodachenko, M. L., Rucker, H. O., Kislyakov, A. G., Zaitsev, V. V., & Urpo, S. 2006, SSRv, 122, 137
Kim, S., Nakariakov, V. M., & Shibasaki, K. 2012, ApJ, 756L, 36
Kliem, B., Karlický, M., & Benz, A. O. 2000, A&A, 360, 715
Kolotkov, D. Y., Broomhall, A.-M., & Nakariakov, V. M. 2015a, MNRAS, 451, 4360
Kolotkov, D. Y., Nakariakov, V. M., Kupriyanova, E. G., et al. 2015b, A&A, 574, 53
Kumar, P., & Cho, K.-S. 2013, A&A, 557, A115
Kumar, P., Innes, D. E., & Inhester, B. 2013, ApJ, 779L, 7
Kumar, P., Nakariakov, V. M., & Cho, K.-S. 2015, ApJ, 804, 4
Kumar, P., Nakariakov, V. M., & Cho, K.-S. 2016, ApJ, 822, 7
Kupriyanova, E. G., Melnikov, V. F., Nakariakov, V. M., & Shibasaki, K. 2010, SoPh, 267, 329
Kuznetsov, A. A., Van Doorsselaere, T., & Reznikova, V. E. 2015, SoPh, 290, 1173
Lang, J., Bentley, R. D., & Brown, C. M. 1992, PASJ, 44, 55
Lemen, J. R., Title, A. M., Akin, D. J., et al. 2012, SoPh, 275, 17
Li, Y. P., & Gan, W. Q. 2008, SoPh, 247, 77
Liefke, C., Fuhrmeister, B., & Schmitt, J. H. M. M. 2010, A&A, 514, 94
Lin, R. P., Dennis, B. R., Hurford, G. J., et al. 2002, SoPh, 210, 3
Linnell Nemec, A. F., & Nemec, J. M. 1985, AJ, 90, 2317
Maehara, H., Shibayama, T., Notsu, S., et al. 2012, Natur, 485, 478
Magee, H. R. M., Güdel, M., Audard, M., & Mewe, R. 2003, AdSpR, 32, 1149
Mariska, J. T. 2006, ApJ, 639, 484
Mason, K. O., Breeveld, A., Much, R., et al. 2001, A&A, 365L, 36
Mathioudakis, M., Bloomfield, D. S., Jess, D. B., Dhillon, V. S., & Marsh, T. R. 2006, A&A, 456, 323
Mathioudakis, M., Seiradakis, J. H., Williams, D. R., et al. 2003, A&A, 403, 1101
McKenzie, D. E., & Mullan, D. J. 1997, SoPh, 176, 127
Mitra-Kraev, U., Harra, L. K., Williams, D. R., & Kraev, E. 2005, A&A, 436, 1041
Mullan, D. J., Herr, R. B., & Bhattacharyya, S. 1992, ApJ, 391, 265
Mullan, D. J., Mathioudakis, M., Bloomfield, D. S., & Christian, D. J. 2006, ApJS, 164, 173
Nakariakov, V. M. 2007, AdSpR, 39, 1804
Nakariakov, V. M., Foullon, C., Myagkova, I. N., & Inglis, A. R. 2010, ApJ, 708L, 47
Nakariakov, V. M., Foullon, C., Verwichte, E., & Young, N. P. 2006, A&A, 452, 343
Nakariakov, V. M., Inglis, A. R., Zimovets, I. V., et al. 2010, PPCF, 52, 124009
Nakariakov, V. M., & Melnikov, V. F. 2009, SSRv, 149, 119
Nakariakov, V. M., Melnikov, V. F., & Reznikova, V. E. 2003, A&A, 412L, 7
Nakariakov, V. M., Pilipenko, V., Heilig, B., et al. 2016, SSRv, 200, 75
Nakariakov, V. M., Tsiklauri, D., Kelly, A., et al. 2004, A&A, 414L, 25
Ning, Z. 2014, SoPh, 289, 1239
Ofman, L., & Wang, T. 2002, ApJL, 580, L85
O'Shea, E., Banerjee, D., Doyle, J. G., et al. 2001, A&A, 368, 1095
Pandey, J. C., & Karmakar, S. 2015, ApJ, 149, 47
Pandey, J. C., & Singh, K. P. 2008, MNRAS, 387, 1627
Pandey, J. C., & Srivastava, A. K. 2009, ApJ, 697L, 153
Pesnell, W. D., Thompson, B. J., & Chamberlin, P. C. 2012, SoPh, 275, 3
Pillitteri, I., Wolk, S. J., Cohen, O., et al. 2010, ApJ, 722, 1216
Pillitteri, I., Wolk, S. J., Lopez-Santiago, J., et al. 2014, ApJ, 785, 145
Pugh, C. E., Armstrong, D. J., Nakariakov, V. M., & Broomhall, A.-M. 2016, MNRAS, 459, 3659
Pugh, C. E., Nakariakov, V. M., & Broomhall, A.-M. 2015, ApJ, 813, 5
Qin, Z., Li, C., Fu, Q., & Gao, Z. 1996, SoPh, 163, 383
Raassen, A. J. J., Mitra-Kraev, U., & Güdel, M. 2007, MNRAS, 379, 1075
Reznikova, V. E., & Shibasaki, K. 2011, A&A, 525A, 112
Robinson, R. D., Carpenter, K. G., & Percival, J. W. 1999, ApJ, 516, 916
Robrade, J., Poppenhaeger, K., & Schmitt, J. H. M. M. 2010, A&A, 513, 12
Robrade, J., Schmitt, J. H. M. M., & Favata, F. 2012, A&A, 543, 84
Rodono, M. 1974, A&A, 32, 337
Ryan, D. F., O'Flannagain, A. M., Aschwanden, M. J., & Gallagher, P. T. 2014, SoPh, 289, 2547
Scandariato, G., Maggio, A., Lanza, A. F., et al. 2013, A&A, 552, 7
Selwa, M., Murawski, K., & Solanki, S. K. 2005, A&A, 436, 701
Selwa, M., & Ofman, L. 2010, ApJ, 714, 170
Shkolnik, E., Walker, G. A. H., Bohlender, D. A., et al. 2005, ApJ, 622, 1075
Simões, P. J. A., Hudson, H. S., & Fletcher, L. 2015, SoPh, 290, 3625
Srivastava, A. K., Lalitha, S., & Pandey, J. C. 2013, ApJ, 778L, 28
Stelzer, B., Schmitt, J. H. M. M., Micela, G., & Liefke, C. 2006, A&A, 460, 35
Stepanov, A. V., Kopylova, Y. G., Tsap, Y. T., et al. 2004, AstL, 30, 480
Stepanov, A. V., Tsap, Yu. T., & Kopylova, Yu. G. 2006, AstL, 32, 569
Strüder, L., Briel, U., Dennerl, K., et al. 2001, A&A, 365L, 18
Sych, R., & Nakariakov, V. M. 2014, A&A, 569, A72
Sych, R., Nakariakov, V. M., Karlicky, M., & Anfinogentov, S. 2009, A&A, 505, 791
Taroyan, Y., Erdélyi, R., Doyle, J. G., & Bradshaw, S. J. 2005, A&A, 438, 713
Trenholme, D., Ramsay, G., & Foley, C. 2004, MNRAS, 355, 1125
Tsiklauri, D., Nakariakov, V. M., Arber, T. D., & Aschwanden, M. J. 2004, A&A, 422, 351
Tsikoudi, V., & Kellett, B. J. 2000, MNRAS, 319, 1147
Turner, M. J. L., Abbey, A., Arnaud, M., et al. 2001, A&A, 365L, 27
Wang, T. 2011, SSRv, 158, 397
Wang, T., Solanki, S. K., Curdt, W., et al. 2002, ApJ, 574L, 101
Wang, T. J., Solanki, S. K., Curdt, W., et al. 2003, A&A, 406, 1105
Watson, C. A., Dhillon, V. S., & Shahbaz, T. 2006, MNRAS, 368, 637
Wilhelm, K., Curdt, W., Marsch, E., et al. 1995, SoPh, 162, 189
Wright, C. S., & Nelson, G. J. 1987, SoPh, 111, 385
Wu, Z., Huang, N. E., Wallace, J. M., et al. 2011, ClDy, 37, 759
Yu, S., Nakariakov, V. M., Selzer, L. A., et al. 2013, ApJ, 777, 159
Yuan, D., Nakariakov, V. M., Chorley, N., & Foullon, C. 2011, A&A, 533, 116
Zaitsev, V. V., & Stepanov, A. V. 1982, SvAL, 8, 132
Zimovets, I. V., & Nakariakov, V. M. 2015, A&A, 577A, 4